BILINGUAL PUBLISHING GROUP

Journal of Environmental & Earth Sciences

https://journals.bilpubgroup.com/index.php/jees

ARTICLE

High-Performance Supercapacitor Electrodes from Optimized Single-Step Carbonized Michelia Champaca Biomass

Dibyashree Shrestha

Department of Chemistry, Patan Multiple Campus, Tribhuvan University, Kathmandu 44613, Nepal

ABSTRACT

This study explores the potential of Michelia champaca wood as a sustainable and locally available precursor for the fabrication of high-performance supercapacitor electrodes. Activated carbons were synthesized through single-step carbonization at 400 °C and 500 °C (SSC-400 °C and SSC-500 °C) and double-step carbonization at 400 °C (DSC-400 °C), with all samples activated using H_3PO_4. The effects of carbonization stratergy on the structural, morphological, and electrochemical characteristics of the resulting carbon materials were systematically evaluated, using techniques such as BET, SEM, TEM, XRD, Raman scattering, FTIR, CV, GCD and EIS. Among the samples, SSC-400 °C exhibited the best electrochemical performance, achieving a specific capacitance of 292.2 Fg^{-1}, an energy density of 6.4 Wh kg^{-1}, and a power density of 198.4 W kg^{-1}. This superior performance is attributed to its optimized pore structure, improved surface functionality and enhanced conductivity. SSC-500 °C showed marginally lower performance, whereas, DSC-400 °C displayed the least favorable results, indicating that double-step carbonization process may negatively affect material quality by disrupting the pore network. This work highlights a strong correlation between synthesis methodology and electrochemical efficiency, directly reinforcing the importance of process optimization in electrode material development. The findings contribute to the broader goal of developing cost-effective, renewable and environmentally friendly energy storage systems. By valorizing biomass waste, the study supports global movements toward green energy technologies and circular carbon economies, offering a viable pathway for sustainable supercapacitor development and practical applications in energy storage devices.

*CORRESPONDING AUTHOR:
Dibyashree Shrestha, Department of Chemistry, Patan Multiple Campus, Tribhuvan University, Kathmandu 44613, Nepal; Email: shresthadibyashree@gmail.com

ARTICLE INFO
Received: 16 January 2025 | Revised: 21 April 2025 | Accepted: 25 April 2025 | Published Online: 16 May 2025
DOI: https://doi.org/10.30564/jees.v7i6.8444

CITATION
Shrestha, D., 2025. High-Performance Supercapacitor Electrodes from Optimized Single-Step Carbonized Michelia Champaca Biomass. Journal of Environmental & Earth Sciences. 7(6): 1–22. DOI: https://doi.org/10.30564/jees.v7i6.8444

Keywords: Michelia Champaca Wood; Activated Carbon; Supercapacitor Electrodes; Carbonization; Sustainable Materials

1. Introduction

Supercapacitors, known for their exceptional power density and rapid charge-discharge capabilities, are critical components in modern energy storage systems. Sustainable activated carbons, with their extensive surface area, well-developed porosity, and high electrical conductivity, are gaining attention as promising electrode materials for these devices [1,2].

Carbon, with its diverse allotropes and tunable electronic properties, stands out as an ideal material for energy storage applications. Its inherent stability, abundance, and environmental friendliness make it a sustainable and attractive choice for developing high-performance energy storage devices [3]. Activated carbons, derived from various precursors through physical or chemical activation processes, possess a hierarchical porous structure composed of interconnected micropores, mesopores, and macropores. This unique architecture facilitates rapid ion transport and efficient charge storage, leading to high specific capacitance and power density. The influence of pore structure on electrochemical performance is well-established; micro and mesopores provide high surface area for charge storage, while larger pores aid in fast ion diffusion, which is critical for enhancing supercapacitor performance.

Michelia champaca, a fragrant hardwood species native to the Himalayan region, including Nepal, offers a sustainable and abundant source for producing high-quality activated carbon electrodes. This species is characterized by its dense structure and high lignin content, which form a robust carbon matrix upon carbonization. Lignin, a complex aromatic polymer, serves as a rich carbon source and supports the development of a well-defined porous structure during activation. The oxygen-containing functional groups, such as hydroxyl and carboxyl groups, present on the surface of the activated carbon, contribute to pseudocapacitance, enhancing the overall electrochemical performance by enabling reversible redox reactions, particularly in aqueous electrolytes.

A key novelty of this study is the introduction of a synergistic Single-Step Carbonization (SSC) approach for producing high-performance activated carbon electrodes from Michelia champaca wood. Unlike conventional methods that involve separate carbonization and activation steps, SSC integrates both processes into a single, efficient step. This approach leverages the high lignin content of Michelia champaca to produce a rigid carbon matrix with a highly porous structure and large surface area, leading to superior energy and power densities in supercapacitors [4–6]. The combination of an optimized single-step process with the specific properties of Michelia champaca represents a novel contribution to the field of sustainable energy storage. The highly optimized pore structure of SSC-derived electrodes, with a balance of micro- and mesopores, facilitates rapid ion diffusion, while the presence of surface functional groups contributes to enhanced pseudocapacitance, allowing for better overall electrochemical performance.

While previous studies have investigated biomass-derived activated carbons for energy storage, this work distinguishes itself by focusing on optimizing the SSC process to achieve exceptional electrochemical performance. By using Michelia champaca, a readily available and sustainable resource in Nepal, this study provides an innovative and practical approach for utilizing local biomass resources. Additionally, it compares the performance of SSC-derived electrodes with those produced using the conventional Double-Step Carbonization (DSC) method [7]. This comparative analysis underscores the novelty of the SSC process and provides valuable insights into its effectiveness for achieving high-performance supercapacitor electrodes.

The objectives of this research are:

1. To prepare activated carbon electrodes from Michelia champaca wood waste using the optimized SSC

method at various temperatures.

2. To characterize the physical and chemical properties of the prepared electrodes, including surface area, pore size distribution, and surface chemistry.

3. To evaluate the electrochemical performance of SSC-derived electrodes in supercapacitor applications, including specific capacitance, energy density, and power density.

4. To compare the performance of electrodes produced by SSC and DSC to determine the optimal method for supercapacitor applications using Michelia champaca as the precursor.

By addressing these objectives, this study contributes significantly to the development of sustainable, high-performance supercapacitor electrodes. The focus on optimizing a single-step carbonization process and utilizing Michelia champaca, an abundant Nepalese hardwood, as a precursor for high-quality activated carbon materials offers a novel pathway for advancing sustainable energy storage solutions.

2. Materials and Methods

2.1. Materials

Michelia champaca wood waste was sourced from local joinery shops in Kathmandu, Nepal. Analytical-grade 85% H_3PO_4, with a specific gravity of 1.73 g mL^{-1} (15.0 M), was purchased from Fischer Scientific, India (P) Ltd. Additional chemicals, including carbon black, polyvinylidene fluoride (PVDF), and N-methyl pyrrolidine (NMP), were procured from Sigma-Aldrich (USA) and APS Ajax Finechem (Australia).

The nickel (Ni) foam substrate used in this study was acquired from PRED MATERIALS International (USA). Ni foam is a widely recognized substrate and current collector in electrochemical energy storage devices due to its unique properties. Its three-dimensional porous structure, lightweight nature, and large surface area provide an excellent platform for the uniform deposition of active materials [8–10]. Additionally, its superior electrical conductivity ensures efficient current collection and distribution, which is critical for enhancing the performance of supercapacitors and other energy storage systems. These characteristics make Ni foam an ideal choice for supporting high-performance electrode materials.

2.2. Methods

Michelia champaca wood waste was collected from local joinery shops in Kathmandu, Nepal, and sun-dried to remove moisture. The dried wood was ground and sieved to achieve a uniform particle size of 100µm. Subsequently, 80 grams of the sieved wood powder was mixed with an equal volume of 85% H_3PO_4 (15.0 M) and soaked for 24 hours at 25 °C using 85% analytical grade H_3PO_4 (Merck, Germany). This 1:1 (w/v) ratio was selected based on prior research findings [11,12], demonstrating its efficacy in producing high-quality activated carbons. To facilitate impregnation, the mixture was heated to 110 °C for 2 hours in a preheated oven.

The synthesis of activated carbon from Michelia champaca wood waste follows a systematic process, as illustrated in **Figure 1**. This includes raw material preparation, chemical impregnation, carbonization at varying temperatures, and post-treatment steps to obtain the final activated carbon samples.

Notably, this study addresses the gap in the literature by exploring Michelia champaca wood waste as a promising precursor for activated carbon electrodes. Unlike commonly used precursors, such as coconut shells or commercial hardwoods, Michelia champaca is a readily available and renewable resource in Nepal, offering an environmentally friendly and low-cost alternative for supercapacitor applications.

2.2.1. Carbonization Methods

Two carbonization methods were employed to optimize the electrochemical properties of the activated carbons:

- Single-Step Carbonization (SSC): The wood powder was thoroughly mixed with phosphoric acid (H_3PO_4) at a 1:1 weight ratio (w/w) without soaking, and the resulting mixture directly carbonized at 400 °C and 500 °C for 3 hours in an inert nitrogen (N_2) atmosphere,

using a controlled heating rate of 10 °C min^{-1}. This method combines carbonization and activation in a single heating cycle, potentially enhancing pore development and surface area due to the synergistic effects of the simultaneous processes [3,12].

- Double-Step Carbonization (DSC): In this method, the wood powder was initially carbonized at 400 °C for 1 hour under N_2, using a heating rate of 10 °C min^{-1}. The carbonized material was then impregnated with phosphoric acid overnight and subsequently carbonized again at 400 °C for 1 hour under N_2, also at a heating rate of 10 °C min^{-1}. This two-step approach enables a more controlled activation process, allowing for the tailoring of pore characteristics. While the single-step carbonization method (SSC) offers a more energy-efficient and cost-effective approach by combining carbonization and activation, the double-step carbonization method (DSC) allows for greater control over the pore structure, potentially leading to more optimized performance. By comparing these methods, we aim to identify the most effective strategy for converting Michelia champaca wood waste into high-performance supercapacitor electrodes.

2.2.2. Post-Treatment

After carbonization, the samples were cooled in air and washed thoroughly with hot distilled water until neutral pH was achieved. The washed samples were dried at 100 °C for 24 hours and ground into fine powders, yielding three activated carbon samples: SSC-400 °C, SSC-500 °C, and DSC-400 °C.

The novelty of this study lies in the comparative investigation of single-step and double-step carbonization methods applied to Michelia champaca wood waste. This dual-method approach offers valuable insights into how processing routes influence pore structure, surface area, and ultimately, electrochemical performance, which is crucial for optimizing energy storage devices.

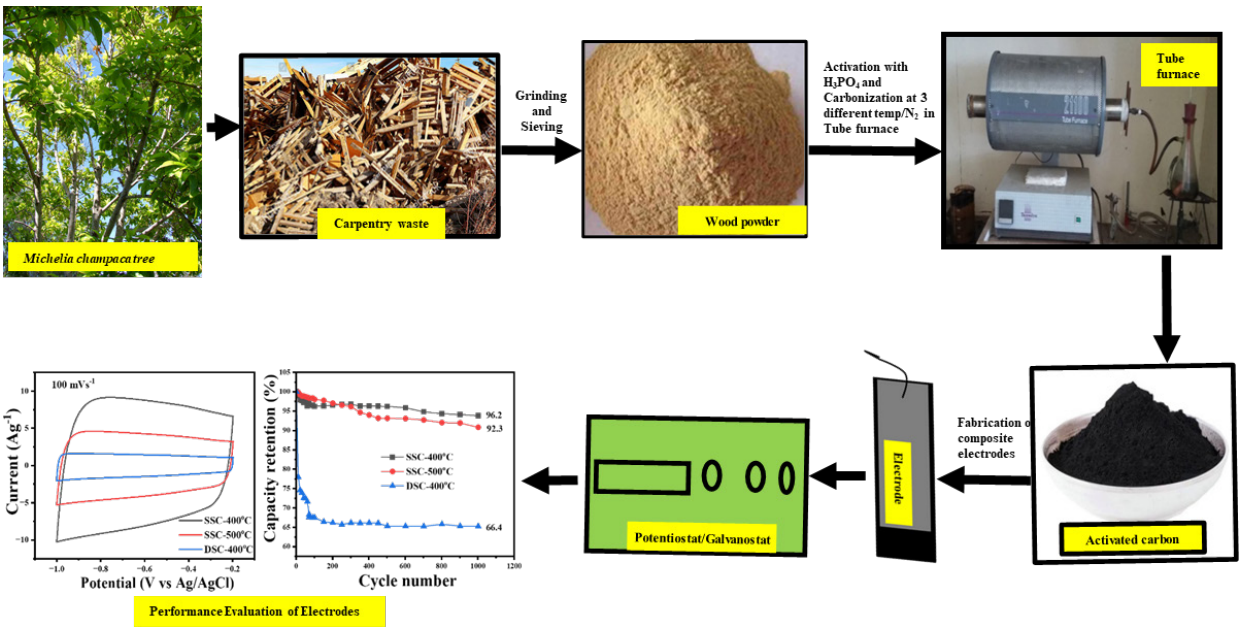

Figure 1. Schematic representation of the synthesis process for activated carbon from Michelia champaca wood waste.

2.3. Characterization

- Thermogravimetric Analysis (TGA): Performed on raw wood powder using an SDT Q600 thermogravimetric analyzer (USA) to study thermal degradation behavior.
- Phase State: X-ray diffraction (XRD) was carried out using a RIGAKU diffractometer (Japan).
- Defect Analysis: Raman spectroscopy was conducted with a labRAM HR800 spectrometer (France).
- Oxygen Content: Fourier Transform Infrared Spectroscopy (FTIR) analysis was performed using a BRUKER-OPTIK GMBH Vertex 70/80 spectrometer (Germany).

• Surface Area and Pore Volume: Determined using a Micromeritics ASAP 2020 system (USA).

• Surface Morphology: Scanning Electron Microscopy (SEM) was conducted using a Mini SEM nanoeyes microscope (Korea).

• Porous Structure: Transmission Electron Microscopy (TEM) analysis was carried out using a JEOL JEM 2100 microscope.

2.4. Assembly of Electrodes

Three distinct electrodes were fabricated as follows:

• Preparation of Electrode Slurry: For each electrode, 8 mg of activated carbon powder (SSC-400 °C, SSC-500 °C, or DSC-400 °C), 1 mg of carbon black, and 1 mg of PVDF were mixed in an 8:1:1 (w/w/w) ratio. The mixture was dispersed in 200 µL of N-methyl-2-pyrrolidone (NMP) to form a homogeneous slurry.

• Electrode Fabrication: The slurry was evenly applied to a 1 cm^2 area of rectangular Ni-foam substrates using the doctor blade technique. The resulting electrode layer had an approximate thickness of 35–40 µm, and the mass loading of active material was around 0.8^{-1}.0 mg cm^{-2}.

• Drying: The coated electrodes were dried overnight at 70 °C to remove the solvent.

• Electrode Activation: Before electrochemical testing, the electrodes were immersed in a 6 M KOH aqueous electrolyte solution overnight. This activation step removed residual impurities and improved wettability and ion accessibility, ensuring stable electrochemical performance [3,4,6].

2.5. Electrochemical Evaluation

The electrochemical performances of the as-fabricated electrodes (SSC-400 °C, SSC-500 °C, and DSC-400 °C) were assessed in triplicate (n = 3) using a three-electrode electrochemical cell in a 6M KOH aqueous electrolyte solution. A platinum (Pt) plate and an Ag/AgCl electrode were employed as the counter and reference electrodes, respectively. All measurements were conducted at room temperature using a Metrohm Autolab (PGSTAT 302 N) potentiostat/galvanostat [4–6].

Cyclic Voltammetry (CV): CV analysis was performed to study the redox behavior and electrochemical reversibility of the electrodes. Measurements were conducted over a potential window of $^{-1}$.0 V to –0.2 V at various scan rates ranging from 2 mV s^{-1} to 100 mV s^{-1}. For clarity, only the CV curve at 100 mV s^{-1} is presented in this manuscript [4-6].

• Galvanostatic Charge-Discharge (GCD): GCD tests were conducted to evaluate the charge/discharge performance and specific capacitance of the electrodes. The tests were carried out at current densities ranging from 1 A g^{-1} to 20 A g^{-1}, with the GCD curve at 1 A g^{-1} included for clarity. Cyclic stability was assessed by measuring capacitance retention after 1000 charge-discharge cycles at a constant current density.

• Electrochemical Impedance Spectroscopy (EIS): EIS measurements were performed to investigate the impedance characteristics of the electrodes. Data were collected by applying a small AC voltage amplitude (10 mV) across a frequency range of 100 kHz to 0.1 Hz. The impedance data were analyzed using Nova 1.11 software to extract key parameters, including charge transfer resistance and solution resistance.

All electrochemical measurements (CV, GCD, and EIS) were performed in triplicate (n = 3), and the reported values represent the average of these measurements to ensure reproducibility and accuracy.

3. Results and Discussion

3.1. Thermal Decomposition of Michelia Champaca Wood Powder

Thermogravimetric analysis (TGA) and differential scanning calorimetry (DSC) were employed to investigate the thermal decomposition behavior of raw Michelia champaca wood powder. TGA measures mass loss during heating, while DSC monitors the heat (enthalpy) flow associated with thermal events. **Figure 2** presents the TGA/DSC plot of raw wood powder.

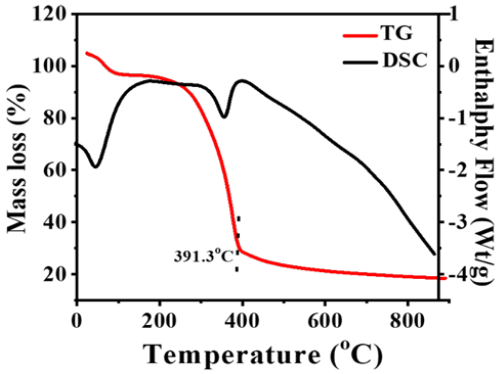

Figure 2. TGA/DSC plot of Michelia champaca wood powder.

3.1.1. Key Observations

- Mass Loss
  - Initial weight loss (0–200 °C): Primarily attributed to the evaporation of moisture and volatile compounds.
  - Major weight loss (200–400 °C): Corresponds to the decomposition of major wood components, including cellulose, hemicellulose, and lignin. A significant exothermic peak at approximately 391.3 °C in the DSC curve indicates intense exothermic reactions during this phase.
  - Residual mass (400–800 °C): The remaining mass at higher temperatures consists mainly of inorganic ash [13,14].
- Enthalpy Flow
  - Exothermic peaks: Observed in the DSC curve, these peaks correspond to the exothermic decomposition reactions of various wood components. The prominent exothermic peak at 391.3 °C is likely associated with the degradation of cellulose and hemicellulose.
  - Endothermic peaks: Minor endothermic peaks may appear at lower temperatures, indicating the absorption of heat during moisture evaporation.

3.1.2. Analysis and Conclusions

- Thermal Stability: The wood powder exhibits moderate thermal stability, with the majority of mass loss occurring between 200 °C and 400 °C.
- Decomposition Mechanism: The presence of multiple exothermic peaks in the DSC curve suggests a complex decomposition process involving the breakdown of different wood components.
- Composition: The residual mass at higher temperatures suggests the presence of inorganic minerals within the wood.
- Energy Content: The significant exothermic peaks observed in the DSC curve indicate that Michelia champaca wood powder possesses considerable heat content, making it a potential source of bioenergy [15].

3.1.3. Carbonization Temperature Selection

The TGA/DSC results demonstrate that the precursor material becomes thermally more stable beyond 400 °C. Based on these findings, 400 °C was selected as the optimal temperature for the carbonization process in this study. This temperature minimizes further mass loss and decomposition while ensuring the removal of volatile components, thereby maximizing the yield of carbonized product [12].

3.2. Structural Analysis of Activated Carbon

3.2.1. XRD and Raman Analysis

Figure 3 shows the XRD and Raman spectra of the three activated carbon samples: SSC-400 °C, SSC-500 °C, and DSC-400 °C. These techniques provide valuable insights into the structural characteristics and potential electrochemical performance of the materials.

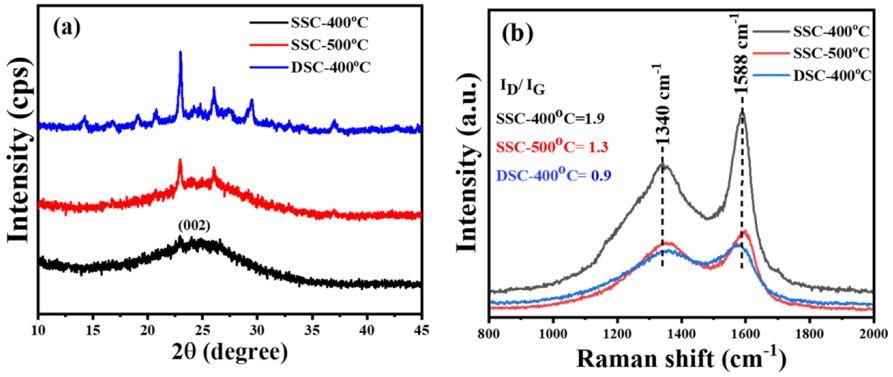

Figure 3. (**a**) XRD pattern and (**b**) Raman spectra of activated carbons.

• XRD Analysis: The XRD patterns (**Figure 3a**) of all three samples exhibit a broad peak centered around 2θ = 25°, characteristic of predominantly amorphous carbon. Additionally, a small, broad peak around 2θ = 25° can be observed, likely associated with the (002) plane of graphitic carbon, suggesting the presence of small, disordered graphitic domains within the carbon structure. This predominantly amorphous nature, enhances ion accessibility and promotes fast electron transport, both of which are beneficial for achieving high capacitive behavior. The XRD patterns exhibit a broad diffraction peak centered around 2θ ≈ 25°, which is characteristic of amorphous carbon due to the lack of long-range order. A very weak and diffuse reflection possibly corresponding to the (002) plane of graphitic carbon may be observed, indicating the presence of only small, disordered graphitic domains. Among the samples, the peak for SSC-400 °C appears broader and less intense, which implies a higher degree of amorphousness compared to SSC-500 °C and DSC-400 °C. This higher amorphous nature is advantageous for supercapacitor applications as it facilitates ion transport and increases surface accessibility.

• Raman Analysis: The Raman spectra (**Figure 3b**) of the samples show distinct D and G bands, confirming their carbonaceous nature. The D band is associated with defects and disorder in the carbon structure, while the G band represents the graphitic structure. The intensity ratio of the D and G bands (ID/IG) reflects the degree of disorder in the carbon materials [16,17].The calculated ID/IG ratios for SSC-400 °C, SSC-500 °C, and DSC-400 °C are 1.9, 1.3, and 0.9, respectively. A higher ID/IG ratio indicates a greater degree of structural disorder or amorphous character.

Accordingly, SSC-400 °C exhibits the highest structural disorder, consistent with its broad amorphous peak in the XRD pattern. The high level of disorder in SSC-400 °C can enhance electrochemical performance by providing more active sites for charge storage and facilitating ion transport within the porous network.

Electrochemical Implications

The higher ID/IG ratio and broader XRD peak of SSC-400 °C confirm its more amorphous nature compared to the other two samples. This disordered carbon structure, while lacking long-range graphitic order, enhances ion diffusion pathways and increases the number of active sites, which is favorable for improving electrochemical performance in supercapacitor electrodes.

Summary

XRD and Raman analyses collectively confirm that SSC-400 °C is the most amorphous among the three activated carbon samples. This greater structural disorder is beneficial for ion accessibility and charge storage [18]. The results align with the superior electrochemical performance observed for SSC-400 °C. Further investigations, including BET surface area and pore structure analyses, are essential to comprehensively understand the structure–performance relationship of these materials.

3.2.2. FTIR Analysis of Activated Carbon Samples

Fourier-Transform Infrared Spectroscopy (FTIR) was employed to identify the presence of functional

groups on the surface of the activated carbon samples. **Figure 4** presents the FTIR spectra of SSC-400 °C, SSC-500 °C, and DSC-400 °C, along with peak assignments and corresponding functional groups.

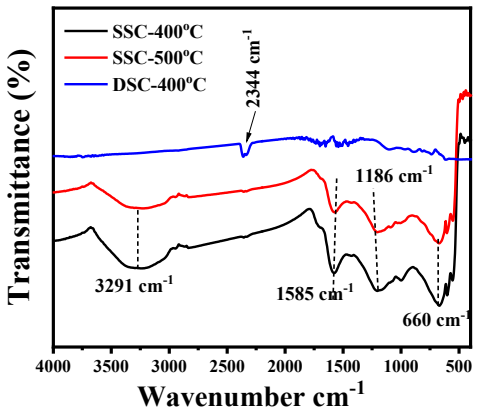

Figure 4. FTIR spectra of activated carbon samples.

Peak Assignments and Functional Groups

- 3291 cm^{-1}: O-H stretching (hydroxyl groups)
- 1585 cm^{-1}: C=C stretching (aromatic rings or double bonds)
- 1186 cm^{-1}: C-O stretching (ether or ester groups)
- 660 cm^{-1}: C-H bending (aliphatic or aromatic hydrocarbons)
- 2344 cm^{-1}: CO_2 absorption

Analysis of Oxygen-Containing Functional Groups

FTIR analysis revealed variations in the concentration of oxygen-containing functional groups across the samples. SSC-400 °C exhibited prominent peaks at 3291 cm^{-1} and 1186 cm^{-1}, indicating the presence of a significant amount of hydroxyl and ether/ester groups [18]. In contrast, SSC-500 °C showed less intense peaks associated with these functional groups, suggesting a decrease in their concentration. DSC-400 °C exhibited minimal or negligible peaks related to hydroxyl and ether/ester groups.

Importance of Oxygen-Containing Functional Groups

Oxygen-containing functional groups, such as hydroxyl and ether/ester groups, play a crucial role in enhancing the electrochemical performance of activated carbon electrodes in supercapacitors. These functional groups can:

- Improve wettability: Enhance the interaction between the electrode material and the electrolyte, facilitating ion transport and charge storage [19,20].
- Contribute to pseudocapacitance: Participate in faradaic reactions, leading to increased charge storage beyond that achieved through double-layer capacitance [19,20].
- Enhance cycling stability: The reversible nature of redox reactions involving surface functionalities can stabilize the charge/discharge process during prolonged cycling.

The stronger presence of such oxygen-rich surface groups in SSC-400 °C suggests a higher degree of pseudocapacitive contribution, which complements its superior specific capacitance and stability observed in CV and long-term cycling data (Section 3.6).

Summary

FTIR analysis revealed that SSC-400 °C possesses a higher concentration of oxygen-containing functional groups compared to SSC-500 °C and DSC-400 °C. These functionalities are closely associated with enhanced electrochemical behavior through improved electrolyte wettability and pseudocapacitive redox contributions. This correlation helps explain the superior performance of SSC-400 °C in terms of specific capacitance and cycling stability, as observed in the electrochemical analyses.

3.3. BET Analysis of Activated Carbon Samples

Figure 5 presents the nitrogen adsorption-desorption isotherms of SSC-400 °C, SSC-500 °C, and DSC-400 °C samples obtained via the Brunauer-Emmett-Teller (BET) method.

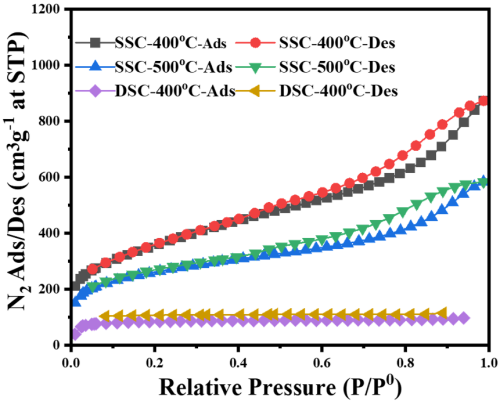

Figure 5. N_2 adsorption–desorption isotherms of activated carbon samples.

3.3.1. Key Observations

- Type I Isotherm: All samples exhibit Type I isotherms, characteristic of microporous materials, indicating dominance of micropores (<2 nm) [21].
- Hysteresis Loops: The presence of hysteresis loops in all samples suggests some degree of mesoporosity (2–50 nm), with SSC-400 °C showing the most pronounced loop, indicating a broader and more accessible pore structure.
- Adsorption Capacity: SSC-400 °C showed the highest nitrogen uptake at P/P° = 1, indicative of its superior surface area and pore volume. **Table 1** summarizes the BET surface area, pore volume, and average pore diameter of the activated carbon samples.

Table 1. BET analysis of activated carbon samples.

Activated Carbons	Specific Surface Area (m^2g^{-1})	Pore Size (BJH Ads) (nm)	Pore Volume (BJH Ads) (cm^3g^{-1})
SSC-400 °C	1894.3	5.4	2.7
SSC-500 °C	1390.4	4.1	1.8
DSC-400 °C	969.2	1.9	0.9

3.3.2. Structure–Performance Correlation

- SSC-400 °C exhibited the highest specific surface area (1894.3 $m^2\ g^{-1}$) and pore volume (2.7 $cm^3\ g^{-1}$) along with a broader pore size distribution (5.4 nm). These characteristics provide a large number of active sites for electric double-layer formation and allow efficient ion diffusion, directly contributing to its superior specific capacitance and rate capability observed in CV and GCD results (Section 3.6).

The presence of both micro- and mesopores in SSC-400 °C ensures an ideal architecture for charge storage: micropores contribute to high capacitance, while mesopores facilitate ion transport, reducing resistance during rapid charge/discharge processes.

- SSC-500 °C while still porous, showed reduced surface area and narrower pores, correlating with moderate electrochemical performance.
- DSC-400 °C, with the lowest specific surface area (969.2 $m^2\ g^{-1}$) and limited mesoporosity, displayed inferior electrochemical behavior due to restricted ion accessibility and slower ion kinetics.

3.3.3. Implications for Electrochemical Performance

- Specific capacitance: Higher surface area and mesoporous character in SSC-400 °C support enhanced charge storage [12,22].
- Rate Capability: Broader pores in SSC-400 °C,

allow faster ion diffusion, which aligns with its stable performance at higher current densities (Section 3.6).

- Charge Transfer Resistance: EIS analysis (Section 3.7) revealed that SSC-400 °C had the lowest charge transfer resistance, which complements the findings of accessible and interconnected pores from BET analysis [23].

3.3.4. Summary

BET analysis confirms that SSC-400 °C possesses a highly favorable porous structure for supercapacitor applications. Its hierarchical pore network and high surface area contribute directly to its superior electrochemical performance by promoting effective ion transport and charge storage [24].

3.4. Scanning Electron Microscopy (SEM) and Correlation with Electrochemical Performance

Scanning Electron Microscopy (SEM) was employed to visualize the surface morphology of the activated carbon samples. **Figure 6** presents the SEM images of SSC-400 °C, SSC-500 °C, and DSC-400 °C.

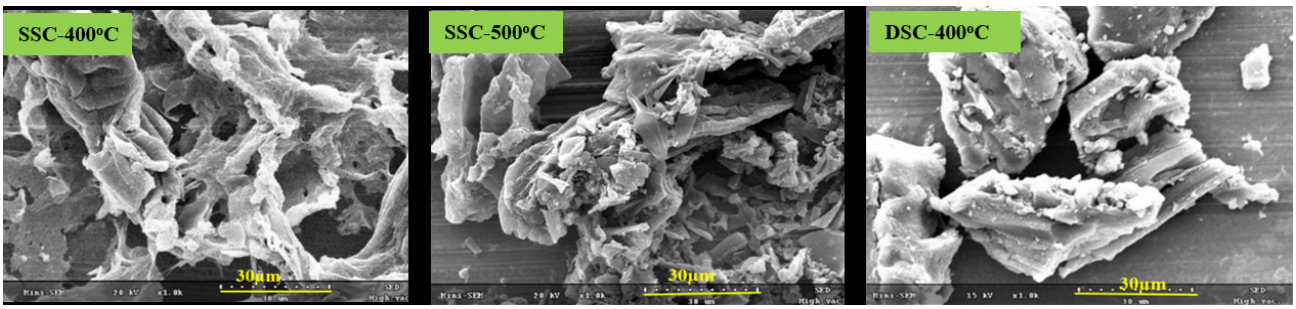

Figure 6. SEM images of activated carbon samples.

3.4.1. SSC-400 °C

This sample shows a rough, heterogeneous surface with numerous visible pores and cracks, indicating a well-developed porous network. Such morphology enhances electrolyte penetration and ion transport, which is consistent with its high specific surface area (1894.3 m^2 g^{-1}) and broad pore distribution observed in BET analysis. FTIR results further suggest the presence of oxygen-containing functional groups contributing to surface roughness. These features collectively explain the superior electrochemical performance of SSC-400 °C, particularly its high specific capacitance and rate capability.

3.4.2. SSC-500 °C

Compared to SSC-400 °C, the surface is smoother with smaller and less interconnected pores. This correlates with the lower surface area and narrower pore distribution in BET analysis, and reduced oxygen functionalities from FTIR. These morphological characteristics likely limit electrolyte diffusion, explaining its relatively reduced capacitance.

3.4.3. DSC-400 °C

The surface appears smooth and compact with minimal porosity. This is consistent with its low BET surface area and weak FTIR signals for surface functional groups. Despite potentially favorable uniform particle distribution, the lack of porosity hinders effective ion diffusion and storage, leading to inferior electrochemical performance.

3.4.4. Overall Implication

The SEM findings reinforce the critical role of surface morphology in governing electrochemical behavior. Specifically, the porous and rough structure of SSC-400 °C enhances wettability, facilitates ion accessibility, and complements its high surface area and functional group content culminating in superior charge storage characteristics.

3.5. Transmission Electron Microscopy (TEM) Analyses

TEM provides high-resolution images of the internal structure, revealing particle size, shape, and distribution (**Figure 7**).

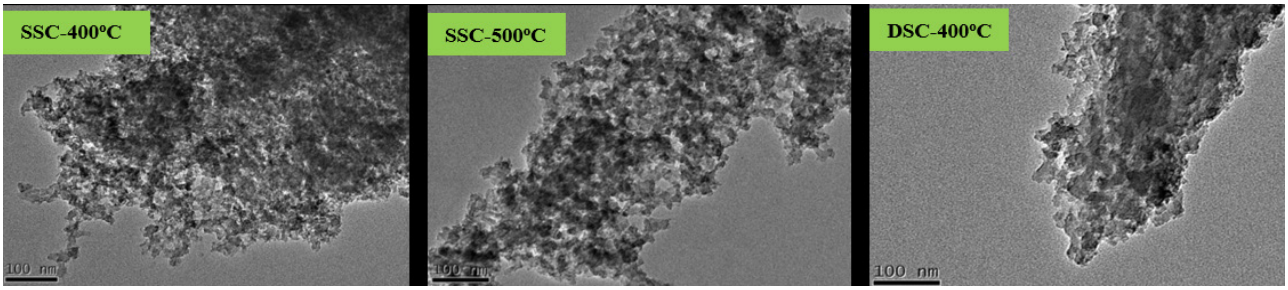

Figure 7. TEM images of activated carbon samples.

3.5.1. Interpretation of the TEM Images

- SSC-400 °C: The structure shows agglomerated particles of varying sizes, with both larger particles and smaller nanoparticles.
- SSC-500 °C: The particles are smaller, more uniformly distributed, and exhibit reduced agglomeration compared to SSC-400 °C.
- DSC-400 °C: The sample displays a uniform distribution of smaller nanoparticles with minimal agglomeration.

3.5.2. Correlating with Previous Analysis

- SSC-400 °C: The agglomerated structure in TEM corresponds with the rough and porous surface observed in SEM, indicating larger particle size and potential agglomeration.
- SSC-500 °C: The smaller, dispersed nanoparticles align with the smoother surface and narrower pore size distribution seen in SEM and BET analyses.
- DSC-400 °C: The uniform nanoparticle distribution matches the compact structure in SEM and the low surface area indicated by BET.

3.5.3. Implications for Electrochemical Performance

- Particle Size: Smaller particles offer a larger surface area for charge storage, enhancing capacitance for high energy density applications [25,26].
- Agglomeration: Excessive agglomeration can hinder ion transport and reduce the effective surface area, negatively affecting performance [27].
- Particle Distribution: Uniform nanoparticle distribution facilitates ion diffusion, improving the rate capability for rapid charge and discharge cycles [28].

3.5.4. Summary

TEM analysis, in conjunction with SEM and BET findings, provides insight into the relationship between particle size, distribution, and electrochemical performance. SSC-400 °C demonstrates the best potential for energy storage applications due to its optimal structure. These insights are valuable for further optimization of activated carbon for supercapacitors and batteries.

The inferior performance of DSC-400 °C may be attributed to the limited structural evolution during the second carbonization at the same temperature, as well as the less effective activation resulting from post-carbonization acid treatment.

3.6. Structural and Morphological Characterization of Activated Carbon Samples for Supercapacitor Applications

A comprehensive structural analysis of the activated carbon samples using XRD, Raman spectroscopy, FTIR, and BET revealed that SSC-400 °C possesses an optimal pore structure and surface area, significantly outperforming the other synthesized materials. While SSC-500 °C displayed comparable characteristics, higher calcination temperatures led to a decline in performance due to pore collapse and structural modifications. In contrast, DSC-400 °C exhibited inferior surface area and unsatisfactory results in SEM, TEM, XRD, Raman, and FTIR analyses. These findings suggest that SSC-400 °C holds exceptional potential for electrochemical applications, particularly in energy storage systems like supercapacitors. To further assess its electrochemical performance, cyclic voltammetry (CV), galvanostatic charge-discharge (GCD), and electro-

chemical impedance spectroscopy (EIS) were conducted.

4. Electrochemical Performances of Activated Carbon Electrodes

4.1. Cyclic Voltammetry (CV)

Cyclic voltammetry (CV) was performed to investigate the electrochemical behavior and charge storage capabilities of the activated carbon electrodes. The CV curves were obtained within a potential window of –1.0 V to –0.2 V vs. Ag/AgCl at various scan rates (2, 5, 10, 20, 50, and 100 mV s^{-1}). For clarity, only the CV curves at a scan rate of 100 mV s^{-1} are presented in **Figure 8**.

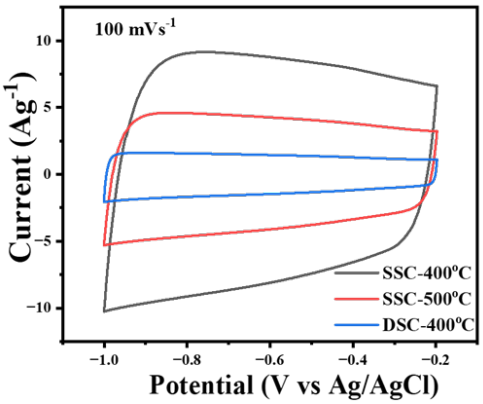

Figure 8. CV curves of activated carbon electrodes at (–1.0 V to –0.2 V).

4.1.1. Capacitive Behavior

The CV curves exhibit a quasi-rectangular shape, indicative of ideal capacitive behavior [12,28], confirming that charge storage primarily occurs through the rapid and reversible adsorption/desorption of ions at the electrode-electrolyte interface.

4.1.2. Current Response

The current response increases linearly with the scan rate, further validating the capacitive behavior of the electrodes.

- SSC-400 °C: Demonstrated the highest current response, indicating the highest specific capacitance.
- DSC-400 °C: Showed the lowest current response, suggesting the lowest specific capacitance.
- SSC-500 °C: Exhibited an intermediate current response, between SSC-400 °C and DSC-400 °C.

4.1.3. Correlation with Other Characterization Techniques

The CV results correlate with the findings from BET, FTIR, and SEM analyses:

- Higher Surface Area: The high capacitance of SSC-400 °C can be attributed to its larger surface area, providing more active sites for charge storage, as shown by BET analysis [27].
- Pore Structure: The broader pore size distribution of SSC-400 °C, observed in BET analysis, promotes faster ion diffusion, contributing to its higher capacitance [28].
- Oxygen-Containing Functional Groups: As indicated by FTIR analysis, the presence of oxygen-containing functional groups may enhance capacitance by contributing to pseudocapacitance [19,20].
- Surface Morphology: The rough and porous surface of SSC-400 °C, observed in SEM images, provides a larger surface area for electrolyte contact, facilitating ion adsorption/desorption [26].

4.1.4. Implications for Electrochemical Performance

The CV results highlight that SSC-400 °C exhibits the most promising electrochemical performance, showing the highest current response and the most ideal capacitive behavior. These results are consistent with other characterization techniques, emphasizing the importance of surface area, pore structure, and surface chemistry in determining the electrochemical performance of activated

carbon electrodes.

4.2. Galvanostatic Charge-Discharge (GCD) Analysis

The GCD curves were obtained for the activated carbon electrodes (SSC-400 °C, SSC-500 °C, and DSC-400 °C) under constant current charging and discharging conditions. The potential response over time is plotted, with time (s) on the x-axis and potential (V vs. Ag/AgCl) on the y-axis [29]. For clarity, only the GCD curves at a current density of 1 A g^{-1} are presented here (**Figure 9**), although additional data were collected at 1, 2, 5, 10, and 20 A g^{-1}.

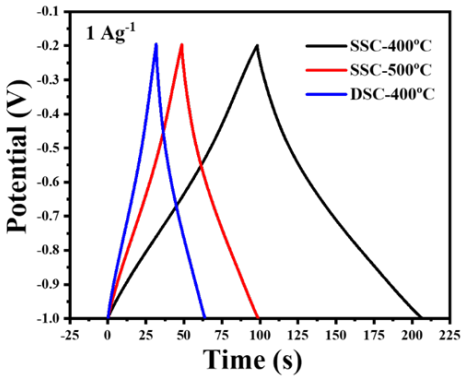

Figure 9. GCD curves of activated carbon electrodes at (–1.0 V to –0.2 V).

4.2.1. Specific Capacitance Calculation

The specific capacitance (Cs) was calculated from the GCD curves using the equation:

$$C_S = \frac{I\Delta t}{m\Delta V} \quad (1)$$

Where,

- Cs (F g^{-1}) is the specific capacitance
- I (A) is the discharge current
- Δt (s) is the discharge time
- m (g) is the mass of the active electrode material
- ΔV (V) is the potential window

4.2.2. Specific Capacitance Results

The specific capacitance values for the activated carbon electrodes were calculated as:

- SSC-400 °C: 292.2 F g^{-1}
- SSC-500 °C: 157.1 F g^{-1}
- DSC-400 °C: 74.3 F g^{-1}

4.3. Rate Capability Evaluation

The rate capability of the activated carbon electrodes was evaluated by examining how the specific capacitance varies with increasing current density. The results are shown in **Figure 10**.

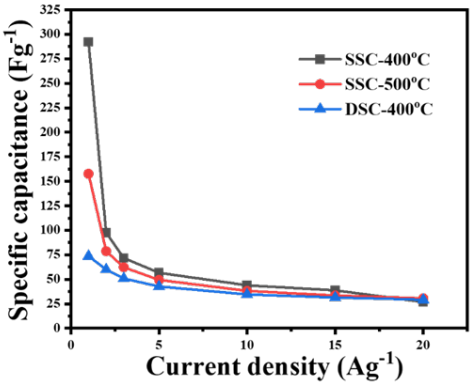

Figure 10. Specific capacitance of activated carbon electrodes vs. current densities.

4.3.1. Key Observations

- Specific Capacitance Trends: SSC-400 °C consistently exhibited the highest specific capacitance across the entire range of current densities, followed by SSC-500 °C and DSC-400 °C.
- Capacitance Decay: A decrease in specific capacitance with increasing current density was observed for all three samples, which indicates diffusion limitations and ohmic losses at higher currents.

4.3.2. Correlations and Implications

- Surface Area: The higher specific capacitance of SSC-400 °C is attributed to its larger surface area, as indicated by BET analysis. The greater surface area provides more active sites for ion adsorption and charge storage.
- Pore Structure: The wider pore size distribution of SSC-400 °C enhances ion transport within the electrode material, improving its rate capability [29].
- Functional Groups: Oxygen-containing functional groups, as detected by FTIR, may contribute to pseudocapacitance, which enhances the overall capacitance [4,12,30].

The GCD results demonstrate that SSC-400 °C exhibits the best rate capability, maintaining a high specific capacitance even at higher current densities. This makes SSC-400 °C a suitable candidate for applications that require rapid charge and discharge cycles, such as pulsed power devices or electric vehicle energy storage systems.

4.3.3. Implications for Electrochemical Performance

The superior rate capability of SSC-400 °C suggests its potential for high-performance supercapacitor applications, especially where fast charge/discharge cycling is crucial. In contrast, DSC-400 °C, with its lower specific capacitance and reduced rate capability, is less suitable for high-current applications.

4.4. Percentage Capacity Retention

The long-term cycling stability of the activated carbon electrodes was assessed by measuring capacity retention over 1000 cycles. The results are presented in **Figure 11**.

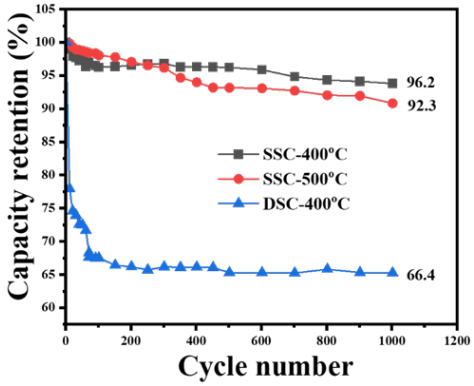

Figure 11. Capacity retention (%) of activated carbon electrodes as a function of cycle number.

4.4.1. Key Observations

- Capacity Fade: All three samples exhibited gradual capacity fade over successive cycles, indicating the challenges of maintaining high capacitance over long-term cycling.
- SSC-400 °C: This sample demonstrated the best capacity retention, maintaining 96.2% of its initial capacitance after 1000 cycles.
- DSC-400 °C: This sample showed the lowest capacity retention, retaining only 66.4% of its initial capacitance after 1000 cycles.
- SSC-500 °C: This sample exhibited an intermediate capacity retention of 92.3% after 1000 cycles, falling between SSC-400 °C (96.2%) and DSC-400 °C (66.4%).

4.4.2. Correlations with Previous Characterizations

- Surface Area and Pore Structure: A larger surface area and wider pore size distribution, as observed in BET analysis, contribute to improved capacity retention by providing more active sites for charge storage and facilitating

ion transport.

- Functional Groups: The presence of oxygen-containing functional groups, indicated by FTIR, likely contributes to the stability of the electrode material and influences its capacity retention.

4.4.3. Summary: Galvanostatic Charge-Discharge (GCD) and Capacity Retention Analysis

- GCD Analysis: SSC-400 °C exhibited the highest specific capacitance (292.2 F g^{-1}) and superior rate capability, making it ideal for applications that demand fast charge/discharge cycles. DSC-400 °C demonstrated the lowest specific capacitance (74.3 F g^{-1}) and poor rate performance.
- Capacity Retention: SSC-400 °C maintained the highest capacity retention, preserving 96.2% of its initial capacitance after 1000 cycles. In contrast, DSC-400 °C retained only 66.4% of its initial capacity, indicating lower long-term stability.

The findings suggest that SSC-400 °C is a promising candidate for supercapacitor applications, offering both high capacitance and excellent cycling stability. These electrochemical performance trends are consistent with the structural and morphological properties of the materials, as indicated by BET, FTIR, SEM, and CV analyses.

- Surface Morphology: The particle size and morphology, as seen in SEM, also affect the long-term stability of the material.

4.4.4. Implications for Electrochemical Performance

SSC-400 °C's superior capacity retention suggests its ability to maintain high performance over extended cycles, making it more suitable for supercapacitor applications where long-term cycling stability is required. DSC-400 °C's lower capacity retention could be linked to its smaller surface area, narrower pore size distribution, and potentially less stable functional groups.

4.5. Electrochemical Impedance Spectroscopy (EIS) Analysis of Activated Carbon Electrodes

Electrochemical impedance spectroscopy (EIS) was employed to investigate the electrochemical behavior of the activated carbon electrodes. This technique, which applies a small-amplitude AC signal to measure impedance across a range of frequencies, provides insights into charge transfer kinetics, diffusional resistance, and interfacial processes [29,30].

4.5.1. Nyquist Plot Analysis

The Nyquist plot illustrates the impedance response of the electrodes (SSC-400 °C, SSC-500 °C, and DSC-400 °C) over a frequency range of 100 mHz to 100 kHz. The x-axis represents the real component of impedance (Z'), while the y-axis depicts the negative imaginary component (−Z″). **Figure 12** shows the Nyquist plots for the three electrodes, highlighting key electrochemical features.

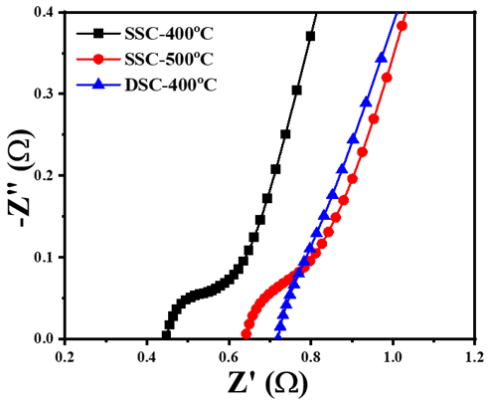

Figure 12. Nyquist plots of activated carbon electrodes.

Key features of the plot include:

- Semicircle in the high-frequency region: This represents the charge transfer resistance (Rct). A smaller semicircle indicates a lower Rct, which is desirable for

better electrochemical performance.

- Sloping line in the low-frequency region: This represents the Warburg impedance (Zw), associated with diffusional limitations. A steeper slope suggests lower diffusional resistance.

4.5.2. Quantitative Analysis

To quantify the Rct and Zw values, the Nyquist plot can be fitted to an equivalent circuit model, such as the Randles circuit. This model consists of a resistor (Rs) representing the electrolyte resistance, a capacitor (Cdl) representing the double-layer capacitance, a resistor (Rct) representing the charge transfer resistance, and a Warburg element (Zw) representing diffusional limitations [25,29].

By fitting the Nyquist plot to the Randles circuit, the values of Rct and Zw can be extracted. The following Table 2 summarizes the extracted values for the three samples:

Table 2. Extracted charge transfer resistance (Rct) and Warburg impedance (diffusional resistance) (Zw) values from Nyquist plot fitting for activated carbon electrodes.

Electrodes	*Rct (Ω)*	*Zw (Ω)*
SSC-400 °C	4.4	6.3
SSC-500 °C	6.3	7.2
DSC-400 °C	7.2	8.1

4.5.3. Interpretation

- Rct: SSC-400 °C exhibits the lowest Rct, indicating the fastest charge transfer kinetics. DSC-400 °C shows the highest Rct, suggesting slower charge transfer.
- Zw: SSC-400 °C also has the lowest Zw, implying the least diffusional limitations. DSC-400 °C exhibits the highest Zw, indicating significant diffusional resistance.
- Overall impedance: SSC-400 °C demonstrates the lowest overall impedance, combining the benefits of low Rct and Zw. This suggests superior electrochemical performance [4,12].

4.5.4. Correlation with Previous Characterizations

The EIS results can be correlated with the findings from other characterization techniques, such as BET, FTIR, SEM, CV, and GCD. For example:

- High surface area: A larger surface area can lead to lower Rct.
- Pore structure: A wider pore size distribution can facilitate ion transport, reducing diffusional resistance.
- Functional groups: The presence of oxygen-containing functional groups can influence the charge transfer kinetics and Rct.
- Particle size and distribution: The surface morphology and particle size distribution can also impact the electrochemical properties.

4.5.5. Summary: Electrochemical Impedance Spectroscopy Analysis

The EIS analysis revealed the charge transfer kinetics and diffusional limitations of the activated carbon electrodes. SSC-400 °C exhibited the lowest charge transfer resistance (Rct) and diffusional resistance (Zw), indicating the fastest charge transfer kinetics and least diffusional limitations. These favorable properties suggest that SSC-400 °C is a promising candidate for supercapacitor applications requiring high power density and good rate capability.

4.6. Power and Energy Density

4.6.1. Ragone Plot Analysis for Activated Carbon Supercapacitors

Figure 13 presents the Ragone plot for the activated carbon electrodes, illustrating the relationship between energy density and power density for SSC-400 °C, SSC-500 °C, and DSC-400 °C. The Ragone plot provides a comparative visualization of energy density (energy stored per unit mass) versus power density (rate of energy delivery). It is an essential tool for evaluating the performance of energy storage devices, including the activated carbon electrodes analyzed here.

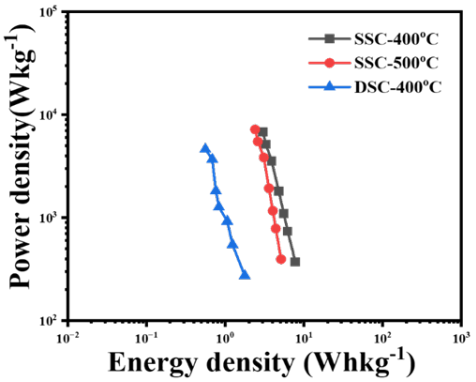

Figure 13. Ragone plot comparing energy density and power density of activated carbon electrodes.

4.6.2. Key Observations

- Performance Positioning: SSC-400 °C occupies the top-right region, signifying superior energy and power densities. In contrast, DSC-400 °C resides in the bottom-left, indicating the lowest performance, while SSC-500 °C lies between the two.
- Energy-Power Trade-off: The expected trade-off is evident, where high energy density often accompanies lower power density and vice versa.

4.6.3. Quantitative Evaluation

The energy density (ED) and power density (PD) were calculated using the following equations:

$$ED = \frac{1}{8} C_{SP} \Delta v^2 \quad (2)$$

$$PD = \frac{E}{\Delta t} \quad (3)$$

In the equations for energy density and power density, the following variables are used:

- V: Potential window (voltage range)
- Δt: Discharge time (seconds)
- ED: Energy density (Wh kg^{-1})
- PD: Power density (W kg^{-1})
- Csp: Specific capacitance (F g^{-1})

In the three-electrode system used, the factor of 8 in the energy density calculation arises due to the specific configuration of the setup. Unlike a two-electrode system where the total capacitance represents the combined contribution of both electrodes, the three-electrode system isolates the working electrode's behavior.

In this configuration:

- The reference electrode monitors the potential of the working electrode without drawing current.
- The counter electrode completes the circuit and balances the current from the working electrode.

This arrangement effectively doubles the capacitance measurement of the working electrode because the counter electrode does not contribute to the capacitance. The energy density equation includes the factor of 8 because energy is proportional to the square of the capacitance. Dividing by 8 ensures that the calculation reflects the true energy storage capability of the working electrode, avoiding overestimation.

By using this adjustment, the energy density values derived from the three-electrode system become directly comparable to those obtained from two-electrode configurations, enabling an accurate evaluation of the material's performance.

4.6.4. Correlation with Material Properties

The Ragone plot findings align with observations from BET, FTIR, SEM, CV, GCD, and EIS analyses:

- Surface Area: A high surface area enhances energy and power densities by increasing active sites.
- Pore Structure: Optimized pore size distribution promotes ion transport, improving rate capability and power density.
- Functional Groups: Oxygen-containing functional groups influence electrochemical behavior, affecting energy and power densities.
- Morphology: Particle size and distribution impact ion accessibility and electrode performance.

4.6.5. Implications for Electrochemical Performance

The Ragone plot confirms SSC-400 °C as the most promising sample, offering a desirable balance of high energy and power densities suitable for supercapacitor applications. In contrast, DSC-400 °C exhibited significantly lower performance, limiting its applicability in high-performance energy storage.

4.6.6. Summary: Ragone Plot Analysis

The Ragone plot analysis highlights SSC-400 °C's superior energy and power densities, positioning it as the top-performing material among the samples. The trade-off between energy and power densities was evident, underscoring SSC-400 °C's potential for applications requiring balanced energy storage and delivery capabilities.

Despite the general assumption that a two-step carbonization process enhances structural development and porosity, in this study, the double-step carbonization (DSC-400 °C) yielded inferior electrochemical performance. This may be attributed to the limited structural evolution during the second carbonization at the same temperature (400 °C), which likely did not induce further pore formation or thermal reorganization. Additionally, performing the acid activation after the initial carbonization may have reduced its effectiveness, as the carbon structure had already begun to consolidate, making it less reactive toward chemical activation. These factors collectively resulted in a lower specific capacitance and energy density, as compared to the single-step process.

4.7. Mechanisms of Enhanced Electrochemical Performance

The superior electrochemical performance of the activated carbon electrodes derived from Michelia Champaca wood using the Single-Step Carbonization (SSC) method can be attributed to a combination of optimized structural features and surface chemistry. These characteristics collectively contribute to enhanced energy and power densities in supercapacitor applications.

4.7.1. Role of Pore Structure

The hierarchical pore structure of SSC-derived electrodes, composed of interconnected micropores, mesopores, and macropores, plays a vital role in their performance. Micropores offer a high surface area for efficient charge accumulation, while mesopores and macropores facilitate rapid ion transport and electrolyte access. This well-developed porosity enables high specific capacitance and fast charge–discharge cycles, which are crucial for practical supercapacitor use. Additionally, the optimized pore size distribution reduces internal resistance and supports ion mobility, thereby enhancing power density.

4.7.2. Contribution of Surface Functional Groups

Surface chemistry, particularly the presence of oxygen-containing functional groups (e.g., hydroxyl and carboxyl), also significantly influences electrochemical behavior. These functional groups contribute to pseudocapacitance through reversible redox reactions at the electrode–electrolyte interface. Beyond double-layer capacitance, this Faradaic contribution enhances overall specific capacitance. Furthermore, these groups facilitate charge transfer, improve cycling stability, and reduce performance degradation over extended use, making the electrodes more reliable for long-term energy storage applications.

4.7.3. Impact of Structural Features on Ion Diffusion Kinetics

The interconnected network of pores in SSC-derived electrodes significantly improves ion diffusion kinetics. The presence of macropores and mesopores provides low-resistance pathways for electrolyte ions, while micropores contribute to charge storage. This synergy ensures rapid ion transport during high-rate charge–discharge cycles, which is particularly beneficial for applications requiring high power output. Enhanced ion diffusion minimizes polarization and improves the rate capability of the device.

4.7.4. Synergistic Effect of Pore Structure and Surface Chemistry

The optimized combination of hierarchical porosity and surface functionalization results in a synergistic enhancement of electrochemical properties. While the structural features ensure fast ion transport and high surface area for charge accumulation, the oxygen-rich surface

chemistry boosts charge retention and enables additional pseudocapacitive storage. This integrated mechanism is responsible for the improved specific capacitance, energy density, power density, and cycling stability observed in SSC-derived electrodes.

4.7.5. Conclusion on Mechanistic Insights

In summary, the enhanced performance of Michelia Champaca-based SSC electrodes arises from a well-coordinated interaction between their physical and chemical features. The hierarchical pore architecture facilitates efficient ion diffusion and charge storage, while surface functional groups introduce Faradaic contributions to the total capacitance. These combined effects make SSC-derived activated carbon electrodes highly promising for next-generation high-performance supercapacitors.

4.8. Comparative Analysis with Previously Reported Biomass-Derived Carbons

To benchmark the electrochemical performance of the SSC-400 °C sample, a comparative analysis was conducted with biomass-derived activated carbons reported in the literature using three-electrode configurations. Table 3 presents key performance parameters such as specific capacitance, energy density, power density, and cycling stability.

Table 3. Comparative performance of SSC-400 °C with other reported biomass-derived activated carbons.

Biomass Precursor	Activation Method	Carbonization Temp (°C)	Specific Capacitance (F g^{-1})	Energy Density (Wh kg^{-1})	Power Density (W kg^{-1})	Cycling Stability (%)	Reference
Michelia champaca (This work)	H_3PO_4 (SSC)	400	292	6.4	198.4	96.2 % (1000 cycles)	This study
Mangifera indica (Mango wood)	KOH	700	284	10.8	750	90% (2000 cycles)	[31]
Teak wood sawdust	KOH	650	300	9.5	720	93% (2000 cycles)	[32]
Dalbergia sissoo (Sheesham)	$ZnCl_2$	600	260	8.5	600	89% (1000 cycles)	[8,33]
Bamboo charcoal	Pyrolysis	600	190	6.8	530	85% (1000 cycles)	[34]

While some previously reported carbons demonstrate slightly higher energy or power densities due to higher carbonization temperatures and stronger/ aggressive activating agents (e.g., KOH, $ZnCl_2$), the SSC-400 °C material offers excellent performance under milder and more environmentally friendly conditions. Furthermore, the use of Michelia champaca as a novel, underutilized biomass precursor adds originality to the present work, supporting its relevance for sustainable and scalable supercapacitor electrode production.

For instance, Hegde and Bhat [31] reported a specific capacitance of 284 Fg^{-1} and an energy density of 10.8 Wh kg^{-1} using activated carbon derived from Mangifera indica leaf waste activated with KOH at 700°C. This comparison highlights the effectiveness of our approach even under less harsh synthesis conditions.

5. Conclusions

This study demonstrates the successful development of sustainable, high-performance, supercapacitor electrode materials by utilizing derived from Michelia champaca wood waste. Activated carbons were synthesized using single-step (SSC) and double-step (DSC) carbonization methods and systematically evaluated through physicochemical and electrochemical techniques including BET, FTIR, SEM, CV, GCD, EIS, and Ragone analysis.

Among the samples, SSC-400 °C showed the most avorable electrochemical properties, confirming its potential as an electrode material for energy storage applications (**Table 4**).

Table 4. Electrochemical properties of the activated carbon samples, including specific capacitance, energy density, power density, charge transfer resistance (Rct), and Warburg impedance (diffusional resistance) (Zw).

Electrodes	Potential Window(V)	Specific Capacitance (Fg^{-1})	Energy Density ($Whkg^{-1}$)	Power Density (Wkg^{-1})	Rct (Ω)	Zw (Ω)
SSC-400 °C	−1 to −0.2	292.2	6.4	198.4	4.4	6.3
SSC-500 °C	−1 to −0.2	157.1	3.5	195.3	6.3	7.2
DSC-400 °C	−1 to −0.2	74.3	1.6	187.3	7.2	8.1

Key performance highlights of SSC-400 °C include:

- **Highest Specific Capacitance (292.2 F g^{-1}):** Indicative of excellent charge storage capability.
- **Superior Energy Density (6.4 Wh kg^{-1}):** Suitable for energy-demanding applications.
- **High Power Density (198.4 W kg^{-1}):** Enables rapid energy delivery.
- **Lowest Charge Transfer Resistance (Rct):** Reflects efficient charge transfer kinetics.
- **Minimal Warburg Impedance (Zw):** Suggests enhanced ion diffusion within the electrode.

In contrast, DSC-400 °C exhibited the lowest performance, while SSC-500 °C demonstrated moderate results, likely due to the effects of higher carbonization temperatures. The study highlights the feasibility of using Michelia champaca, an underutilized biomass, to produce eco-friendly carbon materials for scalable and sustainable supercapacitor applications.

5.1. Scientific Contribution and Broader Implications

This work introduces Michelia champaca as a novel, sustainable biomass precursor for high-performance supercapacitor electrodes. Its successful application demonstrates the untapped potential of underutilized biomass resources in energy storage. Furthermore, the single-step carbonization (SSC) approach proved to be a simple, cost-effective, and environmentally benign method for producing activated carbon. Given its efficiency and reproducibility, the SSC process shows strong promise for broader applicability across other lignocellulosic biomass sources, potentially advancing scalable and green electrode fabrication strategies in next-generation energy storage systems.

5.2. Implications and Future Directions

The results underscore the potential of Michelia champaca-derived activated carbon as a sustainable and efficient electrode material for supercapacitor applications. Among the tested samples, SSC-400 °C demonstrated an excellent balance of high energy and power densities, making it a strong candidate for next-generation energy storage technologies

Future research should aim to:

1. Optimize Synthesis Parameters: Explore tuning the carbonization temperature, heating rate, and activation agent concentration to further enhance material porosity and surface functionalities.
2. Develop Hybrid and Doped Materials: Combine the activated carbon with pseudocapacitive materials (e.g., MnO_2, $Ni(OH)_2$) or introduce heteroatom doping (e.g., N, S) to improve capacitance and charge transfer characteristics.
3. Test in Practical Configurations: Extend electrochemical evaluations to two-electrode systems and examine performance under real-world conditions, including high current densities, varied humidity, and extended cycling tests.
4. Explore Scalability and Integration: Investigate the feasibility of scaling the SSC process and incorporating the material into flexible, wearable, or commercial-grade devices.

By incorporating these advanced directions, the future scope of biomass-derived carbons can be significantly expanded toward high-performance, green, and application-ready supercapacitor technologies.

Funding

This work received no external funding

Institutional Review Board Statement

Not applicable.

Informed Consent Statement

Not applicable.

Data Availability Statement

No new data were created during the study.

Acknowledgements

The author gratefully acknowledges the Central Department of Chemistry at Tribhuvan University, Kirtipur, Nepal, and the Patan Multiple Campus, Institute of Science and Technology, Tribhuvan University, Patan Dhoka, Lalitpur, Nepal, for providing essential laboratory facilities to support this research. Furthermore, the author extends sincere thanks to the Global Research Laboratory (GRL) at Sun Moon University, South Korea, and the Advanced Functional Material Physics (AMP) laboratory at Suranaree University of Technology (SUT), Thailand, for their invaluable contributions in conducting material characterization and electrochemical measurements, respectively.

Conflicts of Interest

The authors declare no conflict of interest.

References

[1] Choi, J.H., Kim, J.E., Lim, G.H., et al., 2020. Comparison of the electrochemical properties of activated carbon prepared from woody biomass with different lignin content. Wood Science and Technology. 54(5), 1165–1180.

[2] Lin, H., Liu, Y., Chang, Z., et al., 2020. A new method of synthesizing hemicellulose-derived porous activated carbon for high-performance supercapacitors. Microporous and Mesoporous Materials. 292(2020), 109707.

[3] Taprial, S., 2015. A review on phytochemical and pharmacological properties of Michelia Champaca Linn. Family: Magnoliaceae. International Journal of Pharmacognosy. 2, 430–436.

[4] Shrestha, D., 2022a. Evaluation of physical and electrochemical performances of hardwood and softwood derived activated carbon for supercapacitor application. Materials Science for Energy Technologies. 5, 353–365.

[5] Shrestha, D., 2022b. Activated carbon and its hybrid composites with manganese (IV) oxide as effectual electrode materials for high performance supercapacitor. Arabian Journal of Chemistry. 15(7), 103946.

[6] Davide B., Toni V., Henrik, R., et al., 2018. Comparison of the properties of activated carbons produced in one-stage and two-stage processes. Journal of Carbon Research. 4(3), 41.

[7] Shrestha, D., 2021. Efficiency of wood-dust of Dalbergia sisoo as low-cost adsorbent for rhodamine-B dye removal. Nanomaterials. 11(9), 2217.

[8] Shrestha, D., 2024. Structural and electrochemical evaluation of renewable carbons and their composites on different carbonization temperatures for supercapacitor applications. Heliyon. 10(5889), e25628.

[9] Shrestha, D., 2023. Applications of functionalized porous carbon from bio-waste of Alnus nepalensis in energy storage devices and industrial wastewater treatment. Heliyon. 9(11), e21804.

[10] Li, X., Liu, J., Chen, J., 2016. Ni-foam as a substrate for energy storage devices: A review, Journal of Materials Science. 51(18), 10431–10452.

[11] Shrestha, D., Rajbhandari Nyachhyon, A., 2021. The effects of different activating agents on the physical and electrochemical properties of activated carbon electrodes fabricated from wood-dust of Shorea robusta. Heliyon. 7, e07917.

[12] Shrestha, D., Maensiri, S., Wongpratat, U., et al., 2019. Shorea robusta derived activated carbon decorated with manganese dioxide hybrid composite for improved capacitive behaviors. Journal of Environmental Chemical Engineering. 7, 103227.

[13] Shrestha, D., Gyawali, G., Rajbhandari, A., 2018. Preparation and characterization of activated carbon from waste sawdust from saw mill. Journal of Institute of Science and Technology. 22(2), 103–108.

[14] Levashov, E.A., Mukasyan, A.S., Rogachev, A.S., et al., 2017. Self-propagating high-temperature synthesis of advanced materials and coatings. International Materials Reviews. 62(4), 203–239

[15] Nurazzi, N.M., Abdullah, N., Norrrahim, M.N.F., et al., 2022. Thermogravimetric analysis (TGA) and

differential scanning calorimetry (DSC) of PLA/cellulose composites. In: Parameswaranpillai, J., Siengchin, S., Salim, N.V. (eds.). Polylactic Acid-Based Nanocellulose and Cellulose Composites. CRC Press: Boca Raton, FL, USA.

[16] Mehdi, R., Naqvi, S.R., Khoja, A.H., et al., 2023. Biomass derived activated carbon by chemical surface modification as a source of clean energy for supercapacitor application. Fuel. 348, 128529.

[17] Xu, L., Jia, M., Li, Y., et al., 2017. High-performance MnO2-deposited graphene/activated carbon film electrodes for flexible solid-state supercapacitor. Scientific Reports. 7(1), 12857.

[18] Yaddanapudi, H.S., Tian, K., Teng, S., et al., 2016. Facile preparation of nickel/carbonized wood nanocomposite for environmentally friendly supercapacitor electrodes. Scientific Reports. 6, 33659.

[19] Kim, J.H., Kim, S.H., Kim, B.J., et al., 2023. Effects of oxygen-containing functional groups on the electrochemical performance of activated carbon for EDLCs. Nanomaterials. 13(2), 262.

[20] Kim, J.-H., Hwang, S.Y., Park, J.U., et al., 2019. Impact of the oxygen functional group of nitric acid-treated activated carbon on KOH activation reaction. Carbon Letters. 29. 281–287.

[21] Shrestha, D., 2022c. Nanocomposite electrode materials prepared from Pinus roxburghii and hematite for application in supercapacitors. Journal of the Korean Wood Science and Technology. 50(4), 219–236.

[22] Li, Y.T., Pi, Y.T., Lu, L.M., et al., 2015. Hierarchical porous active carbon from fallen leaves by synergy of $K2CO^3$ and their supercapacitor performance. Journal of Power Sources. 299, 519–528.

[23] Zhang, J., Yang, H., Huang, Z., et al., 2023. Pore-structure regulation and heteroatom doping of activated carbon for supercapacitors with excellent rate performance and power density. Waste Disposal & Sustainable Energy. 5(3), 417–426.

[24] Goldstein, J.I., Newbury, D.E., Michael, J.R., et al., 2017. Scanning Electron Microscopy and X-ray Microanalysis. Springer: Cham, Switzerland.

[25] Nazhipkyzy, M., Yeleuov, M., Sultakhan, S., et al., 2022. Electrochemical performance of chemically activated carbons from sawdust as supercapacitor electrodes. Nanomaterials. 12, 3391.

[26] Mast, J., Verleysen, E., Hodoroaba, V.D., et al., 2020. Characterization of nanomaterials by transmission electron microscopy: Measurement procedures. In: Hodoroaba, V.-D., Unger, W.E.S., Shard, A.G. (eds.). Characterization of Nanoparticles: Measurement Processes for Nanoparticles. Elsevier: Amsterdam, the Netherlands.

[27] Lv, H., Pan, Q., Song, Y., et al., 2020. A review on nano-/microstructured materials constructed by electrochemical technologies for supercapacitors. Nano-Micro Letters. 12, 1–56.

[28] Ahmad, A., Gondal, M.A., Hassan, M., et al., 2023. Preparation and characterization of physically activated carbon and its energetic application for all-solid-state supercapacitors: A case study. ACS Omega. 8(24), 21653–21663.

[29] Wardani, V., Rohmawati, L., Setyarsih, W., et al., 2019. Analysis of charging/discharging supercapacitor active carbon/rGO based on natural materials. IOP Conference Series: Journal of Physics. 1491(2020), 012044.

[30] Liu, S., Wei, L., Wang, H., 2020. Review on reliability of supercapacitors in energy storage applications. Applied Energy. 278, 115436.

[31] Hegde, S.S., Bhat, B.R., 2024. Sustainable energy storage: Mangifera indica leaf waste-derived activated carbon for long-life, high-performance supercapacitors. RSC Advances. 14(12), 8028–8038.

[32] Jain, A., Jayaraman, S., Ulaganathan, M., et al., 2017. Highly mesoporous carbon from Teak wood sawdust as prospective electrode for the construction of high energy Li-ion capacitors. Electrochimica Acta. 228, 131–138.

[33] Riaz, R., Riaz, M., Mahamood, I., et al., 2017. Evaluation of effect of chemically modified dalbergia sissoo (Sheesham) leaves on biosorption of pb(ii) from aqueous solutions. Oxidation Communications. 40, 898-909.

[34] Yang, C.S., Jang, Y.S., Jeong, H.K., 2014. Bamboo-based activated carbon for supercapacitor applications, Current Applied Physics. 14(12), 1616–1620.